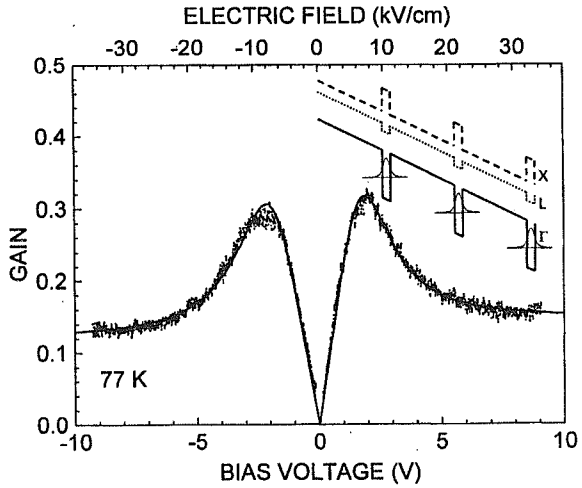

Figure 3: Measured photoconductive gain g (dots) of a 50 period QWIP structure and theoretical fit (solid line) versus applied voltage and electric field. The inset shows the potential distribution of the Γ, L, and X minima in a GaAs/$Al_{0.26}Ga_{0.74}As$ QWIP.

Negative differential photoconductive gain in QWIPs

QWIPs are typically operated at electric fields of the order of 10 kV/cm. This field value is expected to be high enough to induce inter-valley scattering. In order to obtain more information about the transport properties, we have investigated the noise associated with the dark current. The main contribution to the noise current is formed by the generation-recombination (G-R) noise i_{GR}, which is related to the photoconductive gain g and to the dark current I_D by the relation [3]

$$i_{GR}^2 = 4geI_D\Delta f, \tag{5}$$

where Δf is the bandwidth of the measurement. The G-R noise is obtained from the measured noise current i_N via the equation $i_{GR}^2 = i_N^2 - i_{amp}^2 - i_J^2$, which includes small corrections to i_N due to the amplifier noise i_{amp} and the Johnson noise $i_J = (4k_BT\Delta f dI_D/dV)^{1/2}$.

Fig. 3 shows the field dependence of g as obtained from a noise measurement with the QWIP detector covered by a cold shield [12]. At the low-field regime, we observe a strictly linear dependence of g on F up to about ± 5 kV/cm. The linear regime is followed by a strong saturation and, at fields above ± 8 kV/cm, by a pronounced negative differential behavior. For a constant carrier density in the continuum, this negative differential dependence will induce NDC.

Using eq. (1), we now relate g with the drift velocity. Assuming a constant capture time τ_c, eq. (4) allows us to obtain a theoretical fit which is in excellent agreement with the experimental data (see Fig. 3). The fit yields $F_c = 8.0$ kV/cm (9.3 kV/cm) for positive (negative) polarity, $v_v\tau_c = 0.40$ μm (0.32 μm), and $\mu_1\tau_c = 1.57$ $\mu m^2/V$ (1.35 $\mu m^2/V$). Since the value obtained for F_c is only twice as large as in bulk GaAs [11], it is plausible that the observed decrease of g is indeed caused by inter-valley scattering.

Let us now estimate the capture time τ_c. A value of $\tau_c \approx 6$ ps has been predicted previously at $F = 0$ for similar MQW structures [14]. Recent time-resolved photocurrent measurements [15] give rise to a value of $\tau_c < 7$ ps at $|F| > 0$, with a slightly increasing τ_c towards high fields. A field-independent τ_c is therefore a reasonable approximation. Assuming $\tau_c = 5$ ps, the fit yields $v_v = 7.9\text{x}10^6$ cm/s ($6.5\text{x}10^6$ cm/s for negative polarity) and $\mu_1 = 3100$ cm^2/Vs (2700 cm^2/Vs). v_v has a similar value as typically observed in bulk GaAs, while μ_1 is about 3-4 times smaller. The lower value of μ_1 (as compared to bulk GaAs) is in good correspondence with the observed higher value of F_c. The noise gain in Fig. 3 shows a slight asymmetry with respect to the polarity of the bias, which we attribute to an asymmetric distribution of the dopant atoms with respect to the well centers [3, 16].

The potential distributions of the Γ, L, and X-minima are indicated in the inset of Fig. 3. Both the L- and X-minima are expected to contribute to the inter-valley transfer since the L-minimum of $Al_{0.26}Ga_{0.74}As$ lies only slightly below the X-minimum, and since the X-minimum contains the largest density of states. However, the experimentally observed reduction of g at high fields suggests that $\Gamma - L$-transfer is more efficient than $\Gamma - X$ transfer, since the GaAs layers induce shallow wells at the L-point, and potential barriers at the X-point [17]. Therefore, the lowest subbands at the L-point have a much stronger spatial overlap with the GaAs wells than the lowest X-subbands, such that an efficient re-capture into the Γ-point is possible. This interpretation is further supported by the extremely high gain values which have been observed previously in a GaAs/$Al_{0.55}Ga_{0.45}As$ QWIP, where carrier transport occurs mainly at the X-minimum due to the indirect-type AlGaAs barriers [3].

The negative differential behavior of the noise gain in Fig. 3 is in good correspondence with the negative differential behavior of the responsivity observed in Fig. 2. This correspondence is due to the fact that the gain value obtained from the noise measurement can be identified with the gain value associated with the photocurrent. However, clear deviations still exist between the overall bias dependencies observed in both experiments, although the behavior of the responsivity is closer to the noise data for the half-metallized detector than for the completely covered one. The deviations are attributed to different electric field distributions in the dark and under illumination.

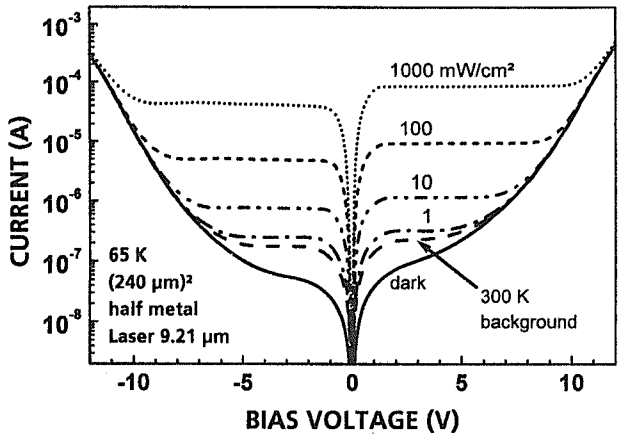

Figure 4: Total current vs. applied voltage at different incident power densities as indicated.

ELECTRIC FIELD DOMAINS

Signature of electric field domains

More information about the transport behavior is obtained at higher excitation densities where the nonlinear transport effects become more prominent. Fig. 4 shows I-V curves measured at different power densities. We have used here half-metallized mesa structures in order to suppress features induced by the interference effect. The data reveal a prominent plateau behavior, which is limited by the mobility regime at low bias (about ± 1.5 V) and by the increase of the dark current at high bias.

Before turning to the discussion of the plateau formation, let us first focus on the behavior of the dark current. As can be seen in Fig. 4, the dark current increases monotonously with applied voltage. This strict increase is due to the fact that the increase of n_{th} with increasing field is more pronounced than the negative differential behavior of $g(F)$, such that the dark current I_D, which is proportional to gn_{th} (see eqs. (1)-(3)), always gives rise to a positive differential conductivity. The strong increase of $n_{th}(F)$ is due to the field-induced reduction of the effective barrier height, which reduces the activation energy of the dark current [3], such that $I_D(F)$ gains an exponential-like behavior at higher fields. From the absence of NDC, we thus expect an approximately homogeneous electric field distribution in the dark.

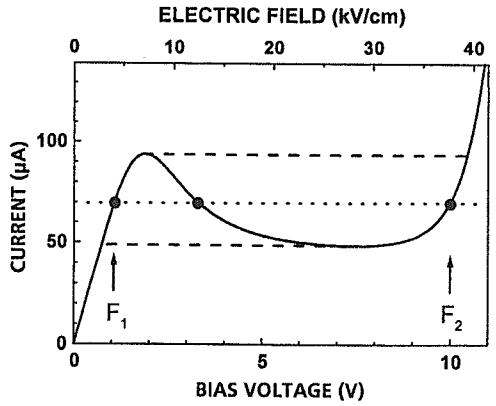

Figure 5: Total current vs. applied voltage as expected in the case of a constant electric field across the MQW structure for $P = 1$ W/cm^2. The full circles indicate the possible local field values (two stable ones and an instable one in between) for a given current indicated by the dotted line. The dashed lines show the regime where multiple fields are possible for a fixed current.

The situation changes drastically when illuminating the device. Here the local photocurrent is directly proportional to g, such that NDC becomes prominent as soon as the total current exceeds significantly the dark current. In Fig. 5, we have plotted the I-V curve as expected for a homogeneous field distribution. Here the photocurrent has been obtained from the measured gain (see Fig. 3), assuming a power density of $P = 1$ W/cm^2 and a quantum efficiency of $\eta = 7\%$, and added to the experimental dark current.

The origin of the plateau formation is as follows. The homogeneous field distribution becomes unstable if the applied field falls into the the NDC regime. On the other hand, two stable field values F_1 and F_2 are possible if the total current is between the peak current and the valley current (between the dashed lines in Fig. 5). Therefore, the field distribution splits up into low-field and high-field domains, characterized by F_1 and F_2, respectively. Since the current, which is already determined by the local field and illumination density within such a domain, is not affected by the domain sizes (as long as the domain field remains constant), this property automatically gives rise to the plateau formation as observed in Fig. 4.

Potential distributions

Potential distributions induced by domain formation are summarized in Fig. 6. The common signature of these distributions consists in the property that the high-

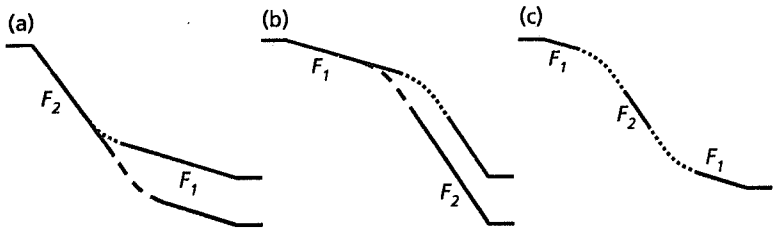

Figure 6: (a) Schematics of stable electric field domains for positive space charge. Upon changing the bias voltage, the transition region (indicated by the dashed and dotted lines, respectively, for two different applied voltages) is shifted while the field values F_1 and F_2 remain constant. (b) Same for a negatively charged transition region. (c) Domain configuration where the high-field domain is located inside the active region.

field domain will increase at the expense of the low-field domain if the applied voltage is increased.

The exact location of the respective electric field domains, as well as the precise value of the plateau current (within the allowed window as indicated by the dashed lines in Fig. 5) is expected to depend on the actual device structure, its structural inhomogeneities, the spatial distribution of the excitation density, and the details of the transport mechanism. A few possible domain configurations are summarized in Fig. 6. In Fig. 6(a), the high-field domain is located adjacent to the emitter contact. This configuration is associated with a positive space charge at the transition region. The opposite case, with the low-field domain close to the emitter contact and a negative space charge, is shown in Fig. 6(b). Finally, a potential distribution containing three domains is sketched in Fig. 6(c). This configuration is accompanied by both positive and negative space charges. Configurations comprising three or more domains are expected to become increasingly probable for longer device structures.

Comparison with electric field domains in other materials

Domain formation is also induced by sequential resonant tunneling in weakly coupled superlattices [18]. A detailed study of the transport properties in this type of domains has been reported recently by Kwok *et al.* [19]. Within a rate equation approach (assuming two domains), they have shown that the current at which domain formation is observed is located significantly below the peak current found in the homogeneous situation. Such a reduction is also expected to occur in the present case when taking into account the microscopic structure of the QWIP, such that the resulting plateau value will be located between the peak and valley currents.

Domain formation in GaAs/AlGaAs superlattices containing a *gradient* in the well widths has been investigated by Han *et al.* [20]. They found that the high-field domain is always formed on the side with the wider well widths, such that the location of the high-field domain does not depend on the polarity of the applied bias.

A similar conclusion has been drawn by Yamashita *et al.* [13], who studied domain formation in *n*-type GaAs. Within their model, the inhomogeneity in the local conductivity is responsible for the location of the high-field domain. Its nucleation is expected to occur at a position where the local electric field has a maximum, which is in turn caused by a local minimum of the conductivity.

We therefore expect that inhomogeneities play a key role for the formation and location of electric field domains in QWIP structures. In this context, inhomogeneities associated with the emitter and collector barriers, as well as inhomogeneities arising from the interference of the infrared illumination (including residual interference in the case of partial metal coverage) are expected to be relevant for the nucleation of high-field domains, rather than structural inhomogeneities within the active region.

CONCLUSIONS

We have shown that the photocurrent in GaAs/AlGaAs QWIPs shows a negative differential behavior, which is attributed to inter-valley scattering. The observation is further substantiated by noise measurements which indicate that the photoconductive gain exhibits the same negative differential dependence, which sets in at an electric field of about 8 kV/cm for a bound-to-extended QWIP. In spite of this negative differential gain, the dark conductivity does not show any anomaly which could be attributed to this effect, since the reduction of the gain is over-compensated by the field-induced increase of the thermal excitation rate.

The field distribution in an illuminated QWIP is strongly influenced by this phenomenon. In fact, the negative differential photoconductivity causes a field distribution which comprises high- and a low-field domains. This phenomenon can be observed already under background-limited operation, such that domain formation may influence the detection properties of QWIP camera systems.

We have also discussed other phenomena giving rise to inhomogeneous electric field distributions. Most importantly, strong interference effects are present in a 45° facet geometry. The resulting spatial dependence of the local excitation density influences significantly the bias dependence of the photocurrent. A convenient way to suppress this interference is obtained by using detector structures in which only half of the top surface is covered with metal.

ACKNOWLEDGMENTS

The authors are grateful to J. Fleissner for sample processing and to P. Koidl and G. Weimann for the encouragement of this study. The work in Freiburg was supported by the Bundesministerium für Verteidigung, Germany.

References

[1]R. Breiter, W. Cabanski, R. Koch, W. Rode, J. Ziegler, K. Eberhardt, and R. Oelmaier, Proc. SPIE **3379**, in press; M. Walther, F. Fuchs, H. Schneider, J. Schmitz, W. Pletschen, J. Braunstein, J. Ziegler, W. Cabanski, P. Koidl, and G. Weimann, Proc. SPIE Vol. **3436**, in press.

[2]S. D. Gunapala, S. V. Bandara, J. K. Liu, W. Hong, M. Sundaram, P. D. Maker, and R. E. Muller, Electrochemical Society Proceedings Vol. 97-33, p. 14 (1997).

[3]B. F. Levine, J. Appl. Phys. **74**, R52 (1993).

[4]M. J. Kane, M. T. Emeny, N. Apsley, C. R. Whitehouse, and D. Lee, Semicond. Sci. Technol. **3**, 722 (1988).

[5]C. Mermelstein, H. Schneider, A. Sa'ar, C. Schönbein, M. Walther, and G. Bihlmann, Appl. Phys. Lett. **71**, 2011 (1997); A. Sa'ar, C. Mermelstein, H. Schneider, C. Schönbein, and M. Walther, IEEE Photonics Technol. Lett. **10**, 1470 (1998).

[6]M. Ershov, H. C. Liu, M. Buchanan, Z. R. Wasilewski, and V. Ryzhii, Appl. Phys. Lett, **70**,414 (1997).

[7]V. D. Shadrin, V. V. Mitin, K. K. Choi, and V. A. Kochelap, J. Appl. Phys. **78**, 5765 (1995).

[8]H. Schneider, C. Schönbein, M. Walther, P. Koidl, and G. Weimann, Appl. Phys. Lett., submitted.

[9]R. W. Ditchburn, "Light" (Academic Press, London, 1976), p. 521ff.

[10]M. Ershov, Appl. Phys. Lett, **72**, 2865 (1998).

[11]B. G. Bosch and R. W. H. Eagelman, *Gunn Effect Electronics* (Pitman Publishing, London, 1975); J. Zongfu and M. Benkun Phys. Rev. **B 44**, 11072 (1991).

[12]H. Schneider, C. Mermelstein, R. Rehm, C. Schönbein, A. Sa'ar, and M. Walther, Phys. Rev. **B 57**, R15096 (1998).

[13]A. Yamashita and R. Nii, Jap. J. Appl. Phys. **5**, 263 (1966).

[14]M. P. Chamberlain and M. Babiker, Semicond. Sci. Technol. **4**, 691 (1989).

[15]S. Ehret, H. Schneider, J. Fleissner, P. Koidl, and G. Böhm, Appl. Phys. Lett. **71**, 641 (1997).

[16]H. C. Liu, Z. R. Wasilewski, and M. Buchanan, Appl. Phys. Lett. **63**, 761 (1993).

[17]P. M. Solomon, S. L. Wright, and C. Lanza, Superlattices Microstruct. **2**, 521 (1986).

[18]K. K. Choi, B. F. Levine, R. J. Malik, J. Walker, and C. G. Bethea, Phys. Rev. **B 35**, 4172 (1987); H. T. Grahn, H. Schneider, and K. v. Klitzing, Appl. Phys. Lett. **54**, 1757 (1989).

[19]S. H. Kwok, H. T. Grahn, M. Ramsteiner, K. Ploog, F. Prengek, A. Wacker, E. Schöll, S. Murugkar, and R. Merlin, Phys. Rev. **B 51**, 9943 (1995).

[20]Z. Y. Han, S. F. Yoon, K. Radhakrishnan, and D. H. Zhang, Appl. Phys. Lett. **66**, 1120 (1995).

GROWTH AND CHARACTERIZATION OF SELF-ASSEMBLED InGaAa/InGaP QUANTUM DOTS FOR MID-INFRARED PHOTOCONDUCTIVE DETECTOR BY LP-MOCVD

Seongsin Kim and Manijeh Razeghi[a]

Center for Quantum Devices, Department of Electrical and Computer Engineering
Northwestern University, Evanston, Illinois, 60208

ABSTRACT

We report InGaAs quantum dot intersubband infrared photoconductive detectors grown by low-pressure metal organic chemical vapor deposition (MOCVD) on semi-insulating GaAs substrates. The InGaAs quantum dots were constructed on InGaP matrix and the optimum growth conditions were investigated. Normal incidence photoconductivity was observed at a peak wavelength of 5.5 mm with a high responsivity of 130mA/W at 77K, and a detectivity of 4.74 x 10^7 cm $Hz^{1/2}$/W at 77K. Low temperature intersubband photoresponse was also observed from the quantum dots grown on Si substrate.

INTRODUCTION

In recent years zero-dimensional quantum devices have received increasing attention since their peculiar characteristics were predicted theoretically.[1] The discovery of self-assembled quantum dots formed by intrinsic strain due to a lattice mismatch has led the research toward rapid development of semiconductor light emitting sources and detectors[2,3,4].

Quantum dot infrared photodetectors are one of the promising applications for semiconductor devices based on zero dimensional quantum structures. There is an increasing need for sources and detectors for mid and far infrared spectral regions due to the broad range of the applications such as IR spectroscopy for chemical analysis, remote sensing, and atmospheric communications. Similar to the case of quantum well intersubband photodetectors (QWIPs), quantum dots are expected to play an important role in infrared photodetectors. Compared to QWIPs, quantum dot detectors has been predicted of the advantages such as a slowing of intersubband relaxation time due to a reduced electron-phonon interaction,[5] high selectivity of the detective wavelength, and temperature insensitivity. In addition, unlike a quantum well, quantum dots are sensitive to the normally incident photons due to the breaking of the polarization selection rules. Recently long wavelength infrared (LWIR) intersubband photoresponse at a peak wavelength of 17 μm from InAs/GaAs,[6] normal incidence LWIR intersubband absorption

[a] razeghi@ece.nwu.edu

INTER-VALLEY SCATTERING AND ELECTRIC FIELD DOMAINS IN QUANTUM WELL INFRARED PHOTODETECTORS

H. Schneider,[1] C. Schönbein,[1] C. Mermelstein,[1,2]
R. Rehm,[1] A. Sa'ar,[2] and M. Walther[1]

[1] *Fraunhofer-Institut für Angewandte Festkörperphysik, Tullastrasse 72, D-79108 Freiburg, Germany*

[2] *Division of Applied Physics, The Fredi and Nadine Herrmann School of Applied Science, The Hebrew University of Jerusalem, Jerusalem 91904, Israel*

We report on the formation of electric field domains induced by the bound-to-continuum photocurrent in n-type GaAs/AlGaAs multiple quantum wells. Domain formation is caused by a negative differential photoconductivity, which arises from inter-valley scattering processes. The domain structure is only observed under illumination, since the thermally excited carrier density increases strongly with increasing electric field, while the optical excitation rate remains constant. The signature of electric field domains, i. e., a plateau-like behavior of the total current under illumination, is most clearly seen if the interference of the infrared illumination is suppressed by using devices which are only partially covered with metal.

INTRODUCTION

Quantum well infrared photodetectors (QWIPs) provide a mature detector technology for thermal imaging cameras. Recently, a 256x256 focal-plane array (FPA) camera based on a GaAs/AlGaAs QWIP sensor has been demonstrated with a noise equivalent temperature difference of less than 10 mK (at an integration time of 20 ms) [1]. Due to this unprecedented thermal resolution, and due to the possibility to realize even much larger (e. g., 640x486 [2]) FPAs with high spatial resolution, QWIP cameras are extremely promising for night vision, early warning systems, medical imaging, etc. Since the system properties are always limited by the performance of the underlying device structure, it is mandatory to know precisely the transport behavior of QWIPs.

In the present paper we focus on the influence of inter-valley scattering on the photoconduction behavior of QWIP structures. We show that inter-valley scattering gives rise to a negative differential photoconductivity, which influences strongly the electric field distribution of the devices in background-limited operation. We also discuss some additional phenomena giving rise to an inhomogeneous electric field

distribution across a QWIP, including the influence of the emitter contact, and spatially inhomogeneous excitation densities due to optical interference of the incident radiation.

EXPERIMENTAL

The QWIP structure under study contains 50 GaAs quantum wells and 51 $Al_{0.26}Ga_{0.74}As$ barriers. The well width is 4.1 nm, Si-doped to a sheet concentration of $4x10^{11}$ cm^{-2} per well, and the barrier width is 48 nm. The active region is sandwiched between n-type GaAs contact layers. The structure was grown by molecular beam epitaxy on a (100)-oriented, semi-insulating GaAs substrate and processed into mesa detectors of 240x240 μm^2 area. The whole mesa area or half of the mesa area, respectively, were covered by an Ohmic contact metallization. The spectral dependence of the photocurrent, as measured with a Fourier spectrometer, shows a peak wavelength of 8.6 μm and a 50% cutoff wavelength at 9.4 μm. The responsivity was measured using the 9.21 μm line of a CO_2-laser, where the measured responsivity (at 2 V applied bias) amounts to 68% of the peak value.

ELECTRIC FIELD DISTRIBUTION IN A QWIP

In this section we give a summary of the main effects which influence the field distribution in a QWIP.

Homogeneous field

In the homogeneous case, the electric field F is constant along the growth axis. The dark current density I_D can be expressed as

$$I_D = e n_{th}(F) v_D(F), \tag{1}$$

with the thermally excited carrier density $n_{th}(F)$ in the continuum and the drift velocity v_D. The responsivity is defined as $R = e\eta g/h\nu$, with the quantum efficiency η, the photon energy $h\nu$, and the photoconductive gain g. At an incident power density P, the total current $I(F)$ is thus given by $I(F) = e n_{th} v_D + RP$. We further have the relation

$$g = v_D \tau_c / L, \tag{2}$$

with the capture time τ_c and the total width L of the active region. The total current can thus be expressed as

$$I = e[n_{th}(F)\frac{L}{\tau_c} + \frac{\eta P}{h\nu}]g(F). \tag{3}$$

Equation (3) is based on the assumption that the photocurrent is associated with the same gain as the dark current. This assumption has been verified previously [3].

In order to explain this behavior, we note that the scattering length of electrons in the continuum (about 50 nm) is about one order of magnitude less than typical drift lengths (usually > 0.5 μm) limited by re-capture into the quantum wells. Therefore, thermally and optically excited electrons in the continuum are expected to have the same energy distribution, such that they are indistinguishable with the same g.

Photo-induced depletion close to the injection barrier

Photo-induced modifications of the field distribution along the active region of a QWIP can be observed if the photocurrent is significantly larger than the dark current. This is, in particular, the case for background-limited detection. Usually, the first quantum well adjacent to the emitter barrier will be partially depleted since electrons are optically excited out of this quantum well, while such excitation does not take place at the GaAs contact layers. This partial depletion is associated with a positive space charge, such that the local electric field across the emitter barrier is higher than the one across the remaining part of the structure. For a stable electric field distribution it is thus necessary that the *thermal* current across the emitter barrier equals the *total* (i. e., thermal and photoexcited) current across the subsequent barrier layer. Such a configuration is always possible since the thermal current increases with increasing electric field. Most of this photo-induced space charge is located at the first well, with a small fraction extended into subsequent quantum well layers.

At a constant applied voltage, the electric field across the emitter barrier is thus enhanced upon illumination, while the field across the remaining part of the QWIP is reduced [5, 6]. This field reduction along the photo-sensitive part of the QWIP gives rise to a corresponding change in the responsivity. We have previously studied the photocurrent nonlinearity in QWIP structures [5]. The nonlinearity turned out to be more pronounced in a QWIP with only 4 periods, where the emitter barrier represents a substantial part of the active region, than in a 50 period device.

Inhomogeneous illumination

Inhomogeneous illumination of a QWIP can be due to several causes. An inhomogeneity already arises from the finite absorption of the detector itself, such that the excitation density is reduced along the direction of light propagation. This effect has been investigated in detail by Shadrin *et al.* [7]. We will neglect its influence in the present paper due to the small quantum efficiency of less than 10% in practical QWIP structures. A spatial variation of the excitation density also occurs in devices supplied with diffraction gratings. An inhomogeneity is induced here since the QWIP structure is located within the transition region between the near-field and the far-field zones of the grating.

A substantial inhomogeneity of the local excitation density of QWIPs is present in devices with 45° facets [8]. The inhomogeneity is caused by the interference be-

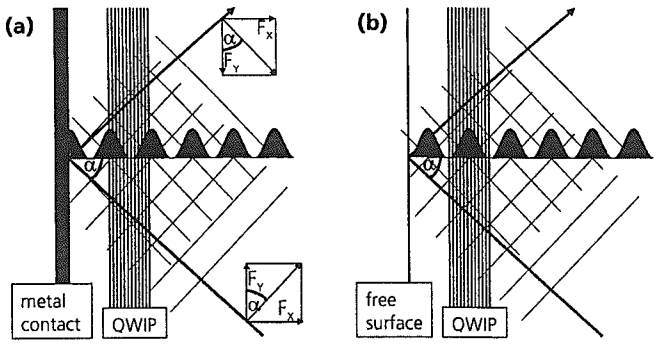

Figure 1: Optical interference of radiation incident at an angle α with respect to the direction normal to a metallized surface (a) and a free surface (b). Vertical lines indicate the quantum wells. Indicated are the wave fronts of the incident and reflected beams, respectively (not to scale). Interference gives rise to an intensity distribution $I_x(x)$ as indicated by the shaded area.

tween the incident and the reflected radiation with the wavelength λ. Assuming a perfectly reflecting metal contact at the surface $x = 0$, the local intensity I_x of the radiation polarized along the growth direction x is proportional to $\sin^2\alpha\cos^2(k_x x)$. Here $\alpha = 45°$ is the angle between the light propagation and the x-axis. $k_x = (2\pi/\lambda)\cos\alpha$ is the x-component of the wave vector. This intensity distribution (with α slightly below 45°) is indicated in Fig. 1(a) for the case of monochromatic illumination. The inhomogeneity will be somewhat reduced for broadband illumination, where the local excitation rate is proportional to the convolution between the light spectrum and the absorption spectrum of the detector.

The inhomogeneity due to interference can be suppressed by using mesa detectors where 50% of the surface area is covered with metal [8]. In fact, a free surface gives rise to a dielectric total reflection, such that we have $I_x \propto \sin^2\alpha\sin^2(k_x x)$. The latter expression is obtained by neglecting the extra phase shift induced by the leakage of the light field into the vacuum, which is a good approximation [9] since α is far from the critical angle for total internal reflection (17°). The resulting spatial distribution of I_x is illustrated in Fig. 1(b). Now, for a 50% metal coverage, the mean power density averaged over the detector area is constant along the growth direction due to the 90 degrees phase shift between the respective interference patterns. Since the in-plane conductivity in the wells is much higher than the conductivity across the barrier layers, each quantum well exhibits in fact a well-defined potential along the

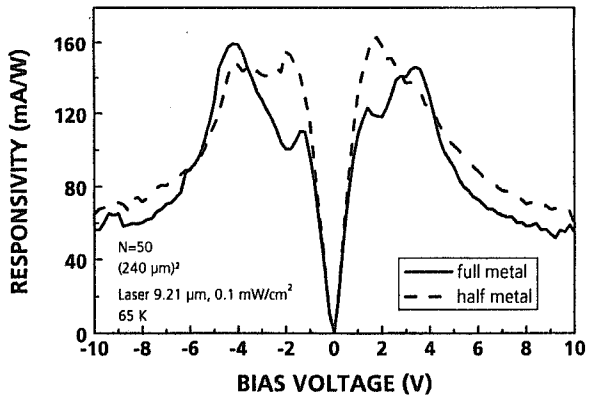

Figure 2: Responsivity vs. applied voltage of a 50-period QWIP with completely metallized (solid line) and with half metallized (dashed line) top contact.

whole area of the detector [10]. Therefore, the half-metallized device should behave in the same way as a device without any interference.

The interference effect has a strong influence on the responsivity if the active region of the QWIP is significantly shorter than π/k_x (which amounts to about 2 μm for $\alpha = 45°$ and $\lambda = 8-9$ μm). In particular, the intersubband absorption of a single quantum well close to the top surface is drastically enhanced upon metal deposition [4].

Fig. 2 shows the bias-dependent responsivity of a 50 period QWIP structure at an excitation wavelength of 9.21 μm, for mesa devices with full and half metal coverage of the top surface, respectively. The measurement was performed with a lock-in technique at a small excitation density of 0.1 mW/cm^2, which is more than an order of magnitude lower than the intensity of the thermal 300 K background radiation incident on the devices. The responsivity shows different voltage dependencies for the two configurations. The fully metallized device has its highest responsivities at -4.2 V and +3.4 V, while the half-metallized structure has its peak values at -2 V and +1.8 V.

The influence of the metal coverage of the top surface on the voltage dependent behavior of the QWIP can be understood qualitatively from equation (3). If the excitation density P is spatially modulated due to an interference pattern as shown in Fig. 1(a), then the electric field will also gain a dependence on the coordinate x, such that the total current I in equation (3) is conserved. In the regime where g

depends only weakly on F (or where n_{th} depends much more strongly on F than the gain g), n_{th} thus has to decrease with increasing local power density $P(x)$. This means that regions with high $P(x)$ are associated with low $F(x)$ (and vice versa), since n_{th} is known to increase strictly with increasing F. Therefore, at a constant applied bias, the local electric field at the "dark" regions will increase at the expense of the field at the illuminated parts of the active region. A strong spatial variation of $P(x)$ will thus give rise to a local electric field at the illuminated regions which is smaller than for homogeneous illumination and smaller than the externally applied field. It is due to this field reduction why the highest responsivity of the fully-metallized detector is observed at larger bias voltages than in the half-metallized case.

In spite of the strongly different bias dependencies, the overall responsivity values are similar for the two devices. This is due to the fact that the length of the active region has a similar value as π/k_x, such that the average excitation density within the total excitation *volume* is approximately identical for the two detectors.

The data in Fig. 2 show additional features, including negative differential photoconductivity, which cannot be explained in terms of inhomogeneities or contact effects. The following section will set the basis to explain some of these structures.

INTER-VALLEY SCATTERING

Negative differential conductivity and the Gunn effect in III-V semiconductors

In most III-V bulk semiconductors, negative differential conductivity (NDC) is observed in n-type material at sufficiently high electric fields (e. g., at $F > 5$ kV/cm in GaAs). This NDC is induced by scattering of the carriers from the Γ-minimum into the L- and X-minima of the conduction band. These inter-valley scattering processes give rise to a reduced conductivity since, due to the higher effective mass, the electron drift velocity at an indirect minimum is smaller than at the Γ-point. In GaAs, the negative differential dependence of the average drift velocity v_D as a function of the electric field F is well described by the expression [11]

$$v_D(F) = \frac{\mu_1 F + v_v (F/F_c)^4}{1 + (F/F_c)^4}, \tag{4}$$

where μ_1 is the mobility at the Γ-point, v_v the asymptotic drift velocity for $F \to \infty$, and and F_c the characteristic field for inter-valley scattering.

The NDC gives rise to the formation of stable electric field domains at small carrier densities (typically $< 10^{14}$ cm^{-3}) [13]. Propagating domains are observed at higher carrier densities. In the latter case, pronounced oscillations of the current are observed [11]. These Gunn-oscillations have found widespread use in microwave oscillators and amplifiers.